Quantifying the uncertainty in forecasts of anthropogenic climate change

Myles R. Allen*, Peter A. Stott†, John F. B. Mitchell†, Reiner Schnur‡ & Thomas L. Delworth§

** Space Science and Technology Department, Rutherford Appleton Laboratory, Chilton, Didcot OX11 0QX, UK*
† Hadley Centre for Climate Prediction and Research, The Meteorological Office, London Road, Bracknell RG12 2SZ, UK
‡ Max-Planck-Institut für Meteorologie, Bundesstrasse 55, 20146, Hamburg, Germany
§ Geophysical Fluid Dynamics Laboratory/NOAA, PO Box 308, Princeton, New Jersey 08542-0308, USA

Forecasts of climate change are inevitably uncertain. It is therefore essential to quantify the risk of significant departures from the predicted response to a given emission scenario. Previous analyses of this risk have been based either on expert opinion[1], perturbation analysis of simplified climate models[2–5] or the comparison of predictions from general circulation models[6]. Recent observed changes that appear to be attributable to human influence[7–12] provide a powerful constraint on the uncertainties in multi-decadal forecasts. Here we assess the range of warming rates over the coming 50 years that are consistent with the observed near-surface temperature record as well as with the overall patterns of response predicted by several general circulation models. We expect global mean temperatures in the decade 2036–46 to be 1–2.5 K warmer than in pre-industrial times under a 'business as usual' emission scenario. This range is relatively robust to errors in the models' climate sensitivity, rate of oceanic heat uptake or global response to sulphate aerosols as long as these errors are persistent over time. Substantial changes in the current balance of greenhouse warming and sulphate aerosol cooling would, however, increase the uncertainty. Unlike 50-year warming rates, the final equilibrium warming after the atmospheric composition stabilizes remains very uncertain, despite the evidence provided by the emerging signal.

Many attempts have been made to forecast the response of the climate system to anthropogenic changes in atmospheric composition. For example, the first five squares in Fig. 1 (from left to right) show predicted global mean temperature in the decade 2036–46 relative to the pre-industrial (control) climate for four atmosphere–ocean general circulation models (A–OGCMs)[12–15] all driven with approximately the same scenario (IS92a, ref. 16) of greenhouse gas and sulphate aerosol (GS) concentrations. (The fourth square is from a model that includes the effects of indirect sulphate and tropospheric ozone concentrations[14].)

A basic problem with all such predictions to date has been the difficulty of providing any systematic estimate of uncertainty. Predictions in Fig. 1 range from 1.1 to 2.3 K, but translating inter-model spread into an objective uncertainty range is problematic because these models do not necessarily span the full range of known climate system behaviour. Their climate sensitivities (equilibrium warming on doubling carbon dioxide), for example, all lie in the range 2.5–3.5 K: a smaller range than even the most optimistic current estimate of uncertainty in this parameter. Other A–OGCMs exist with sensitivities outside this range, but a probabilistic interpretation of the spread of 'current' predictions is inevitably subjective.

An alternative approach is illustrated by the heavy solid line in Fig. 2. This shows how the predicted warming by 2036–46 under the IS92a GS scenario varies with the simulated rate of anthropogenic warming over the twentieth century as we vary the prescribed climate sensitivity in a simple climate model[2]. The plot is close to a straight line through zero, indicating a simple linear relationship between the amplitude of the signal observed to date and the size of mid-twenty-first-century warming. Almost the same relationship emerges if we assume a different rate of oceanic heat uptake[17] (heavy dotted line). Thus, if the range of twentieth-century warming trends attributable to anthropogenic influence were 0.25–0.5 K per century, this model suggests that the uncertainty range in 2040s temperatures would be 1–2 K, irrespective of the accuracy of the model's climate sensitivity or rate of oceanic heat uptake.

In contrast, the relationship between the observed signal and the equilibrium climate sensitivity is both nonlinear and dependent on the assumed rate of oceanic heat uptake. A range in recent anthropogenic warming rates of 0.25–0.5 K per century would translate into an uncertainty in sensitivity of 1.5–4 K if we assume the faster rate of oceanic heat uptake (thin dotted line in Fig. 2, right-hand scale). With the slower rate (thin solid line), no useful upper bound could be placed on the climate sensitivity on the basis of twentieth-century temperature trends. Thus we cannot estimate climate sensitivity from recent observed surface temperature trends without an independent estimate of the rate of oceanic response[2,5,17]. Even if this response time were known, if it turns out be towards the slower end of the current uncertainty range, then it may still be impossible to provide a useful upper bound on climate sensitivity on the basis of recent trends.

We expect similar relationships to those in Fig. 2 to hold in more complex systems, provided both the strength of atmospheric feedbacks and the rate of oceanic heat uptake do not change in response to perturbations of this magnitude. The fact that most A–OGCMs give an almost linear response to a linear increase in radiative forcing[6] provides support for this assumption, but direct perturbation analysis of more complex models with realistic forcing trajectories is required to explore fully its validity[18].

Considering only the transient response, the problem now becomes: what fraction of the recent observed warming should be attributed to anthropogenic influence? Climate change detection

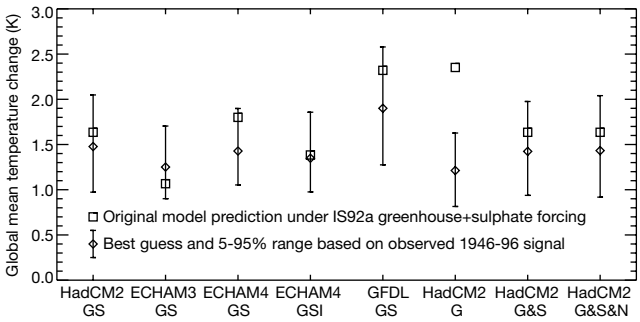

Figure 1 Predicted anthropogenic warming by about 2040 under the IS92a scenario before and after reconciling model simulations with the recent climate record. Squares, temperature change relative to pre-industrial (control) climate in a range of climate models for the decade 2036–46 under the IS92a scenario of greenhouse gas and sulphate (GS) forcing (greenhouse gas only in sixth case, G). Diamonds, scaled temperature change after reconciling model-simulated large-scale patterns of near-surface temperature anomalies (taken about the 1896–1996 mean) over the five decades 1946–96 with the corresponding observed signal using an optimal fingerprint algorithm. First six cases, scaling single GS or G simulation; seventh case, net anthropogenic warming estimating greenhouse gas and sulphate responses independently; eighth case, net anthropogenic warming estimating greenhouse gas, sulphate and natural (combined solar and volcanic) signals independently, assuming no naturally forced change after 1996. Vertical bars, uncertainty in the scaled response based on uncertainty in the scaling factor(s) required to reconcile the models with observed changes.

techniques[19,20] provide an estimate of this fraction or, more specifically, an estimate of the factor by which we have to scale a model-simulated trajectory to match the magnitude of the observed anthropogenic signal[20], together with an objective estimate of the corresponding range of uncertainty.

The first five diamonds in Fig. 1 show the various models' predictions for total warming by 2036–46 under the IS92a GS scenario after scaling their respective trajectories to match the amplitude of observed near-surface temperature anomalies (relative to the 1896–1996 mean) over the 1946–96 period. By the mid-twenty-first century, sampling uncertainty in the raw model predictions is small relative to the climate change signal, particularly if ensemble simulations are available. Thus a factor-of-two uncertainty in the scaling required on the model-simulated twentieth-century response translates into a factor-of-two uncertainty in the scaled prediction.

Rather than simply using temperature trends as a measure of the strength of the observed signal, we use a full spatio-temporal "fingerprint"[19] of the various responses[11,21]. This provides an "optimal estimate"[10] of the scaling required to match the amplitude of the observed signal[20], minimizing uncertainty due to internal climate variability. Application of this scaling improves inter-model consistency, with predictions from un-responsive models being scaled up and predictions from highly responsive models scaled down. The GFDL model prediction remains higher than the others, implying that the A–OGCMs are diverging by more than we would expect if they were simply providing scaled versions of the same underlying trajectory. The further we predict into the future, the greater this divergence is likely to be, so our approach is only valid over timescales up to the length of the observational record used. Estimated uncertainties in the amplitude of the scaled response, based on the individual models' estimates of internal climate variability, are shown by the vertical bars.

To show what happens if an important process is omitted, the sixth square in Fig. 1 shows the predicted warming by 2036–46 from the HadCM2 model forced with rising greenhouse gases alone. The raw prediction is over half a degree warmer than the same model under GS forcing, but the fingerprint analysis suggests that this model trajectory would need to be scaled down significantly to be consistent with recent observations. After such scaling, the resulting best-guess and uncertainty range is in better agreement with the GS simulations. This point is important because other processes may also have been omitted from all the GS simulations. Provided these processes have a proportionally similar impact on the signal observed to date as on early twenty-first-century warming (as would be the case for an atmospheric feedback that scales approximately linearly with the surface temperature change), their omission from the models would not affect the estimated scaled prediction.

Errors which only show themselves in the future, such as a failure to represent a sudden shut-down in the thermohaline circulation, would not be accounted for in this analysis. Most currently simulated circulation changes seem to be relatively gradual over the timescales of interest[22], but the possibility of sudden nonlinear climate change limits the forecast lead time over which this approach can be pursued. The assumption that the spatio-temporal patterns of response are independent of the response amplitude appears to be acceptable for large-scale surface temperature changes[8], but it would not be valid for changes in precipitation[23] or atmospheric circulation[24], or for cases in which the forcing changes abruptly over the period of interest.

Another assumption underlying the first five bars in Fig. 1 is that the relative amplitude of the responses to greenhouse gases and to sulphate aerosols is as simulated in these GS experiments, so the combined response can be represented in each case by a single spatio-temporal pattern. Given the considerable uncertainty in the sulphate forcing and response, this is difficult to justify. For the HadCM2 climate model, we have separate multi-member ensemble simulations of the greenhouse-gas-only (G) and the GS response. The fingerprinting approach allows separate estimates of the amplitude of both the greenhouse and sulphate signals in the observations, together with their joint uncertainty range[9,19,20]. By scaling

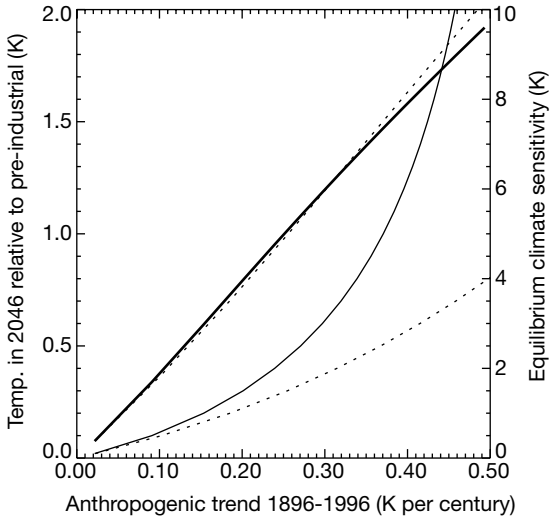

Figure 2 Transfer functions relating past and future climate change in a simple climate model. Heavy solid line, left-hand scale: relationship between simulated global mean temperature trends over the period 1896–1996 and the predicted total anthropogenic warming by the decade 2036–46, obtained by varying the climate sensitivity in a simple climate model[2] under IS92a greenhouse and sulphate forcing. Heavy dotted line, relationship obtained assuming a different rate of oceanic heat uptake (effective vertical diffusivity of 0.25 $m^2 s^{-1}$ versus 2.0 $m^2 s^{-1}$ in the base case). Light solid and dotted curves, right hand scale: corresponding relationships between simulated 1896–1996 temperature trends and equilibrium climate sensitivity.

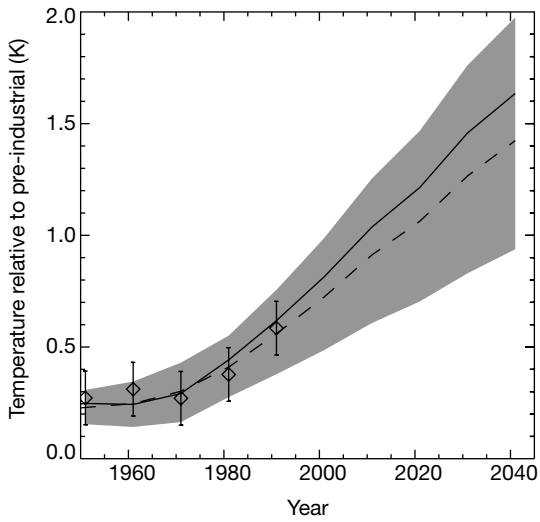

Figure 3 Global temperatures under IS92a consistent with the recent climate record. This figure shows simulation and forecast of decadal global mean temperatures relative to pre-industrial (control) values as predicted by HadCM2 under the IS92a GS scenario. Solid line, mean of original 4-member ensemble simulation. Dashed line, after scaling the model-simulated spatio-temporal patterns of response to greenhouse gas and sulphate forcing individually to give the best combined fit to the observations over the 1946–96 period. Shaded band, 5–95% confidence interval on scaled response. Diamonds, observed decadal global mean temperatures (anomalies about the 1896–1996 mean, added for display to the corresponding mean of the GS ensemble); vertical bars, ±2 s.d. of decadal mean temperatures from HadCM2 control.

their individual contributions to model-predicted future warming accordingly, we arrive at an uncertainty estimate which does not depend on the amplitude of the model-simulated response to either forcing agent.

The seventh bar in Fig. 1 shows the resulting range of uncertainty in the HadCM2 prediction for 2036–46, while Fig. 3 shows how this uncertainty range evolves over time. The solid line shows the original model prediction; the dashed line and shaded band show the median and 5–95% uncertainty range after scaling the simulated greenhouse and sulphate signals to match observed large-scale temperatures over the 1946–96 period. The observed spatially-averaged global mean temperatures of the five decades 1946–1996 are shown (diamonds) for illustration only: scaling factors are estimated from the full spatio-temporal pattern of temperature change. The figure shows the range of uncertainty in the underlying anthropogenic trend: superimposed on this would be uncertainty due to internal variability, indicated by the vertical bars on the observations, and due to other forcing agents.

Estimating separately the amplitudes of greenhouse and sulphate signals does not appear to increase forecast uncertainty: the first and seventh bars in Fig. 1 are almost identical. The reason is that the combination of greenhouse warming and sulphate cooling predicted under the IS92a emissions scenario happens to be particularly well constrained by the observed signal at the global level. This is shown in Fig. 4, which focuses on warming over the coming 50 years rather than warming relative to pre-industrial times as shown in Figs 1–3. The dotted contours show how projected warming over the five decades to 2046 depends on the scaling factors applied to the model-simulated greenhouse and sulphate signals. The raw model prediction is a greenhouse warming of 1.35 K and a sulphate cooling of 0.35 K over this period, giving a net warming of 1 K assuming both scaling factors are unity (the square). If we scale the sulphate signal up or down by a factor of 1.35/0.35 faster than we scale the greenhouse signal (that is, moving along an isoline of future warming), the net warming 1996–2046 is unchanged.

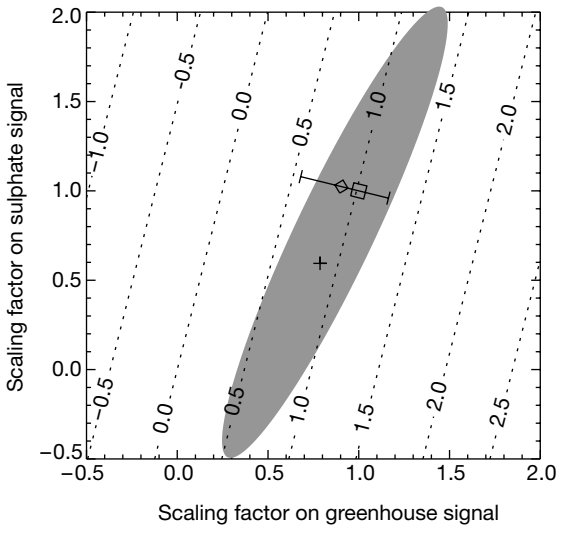

Figure 4 Forecast anthropogenic warming 1996 to 2046 under IS92a. Dotted contours, isolines of global mean warming (in K) between the decade 1986–96 and the decade 2036–46 as a function of the scaling factors applied to the raw HadCM2 prediction of a 1 K warming (square). Cross and shaded region, best-guess and joint 90% confidence region on estimated scaling factors required to reproduce observed large-scale near-surface temperatures over the 1946–96 period using response-patterns simulated by HadCM2. Diamond and solid error bar, best-guess and 5–95% range on forecast warming (read off from the contours) obtained by a probability-weighted sum of 'allowed' scaling factors along the isolines of future warming. The error bar is superimposed on the raw prediction (square) for comparison with Fig. 1: provided the diamond and cross lie on the same isoline of future warming, its location is otherwise arbitrary.

The cross and shaded region show the best guess and joint 90% uncertainty range on the scaling factors required on the model-simulated greenhouse and sulphate response-patterns to reproduce observed temperatures over the 1946–96 period. The uncertainty range is strongly tilted, meaning the model could over- (or under-) estimate the magnitude of recent greenhouse warming and still be consistent with the observed signal provided it also over- (under-) estimates the magnitude of sulphate cooling. The principal axis of the uncertainty region is close to parallel to the isolines of future warming, so uncertainty in predicted 50-year warming under the IS92a scenario is relatively low (the best-guess of 0.9 K and the 5–95% range of 0.55–1.2 K are shown by the diamond and the solid bar).

Any reduction in future sulphate cooling not only increases the best-guess net future warming, but it also substantially increases the uncertainty range consistent with current observations. The reason is that the two-dimensional confidence region would no longer be so well aligned with the isolines of predicted warming. For example, if the predicted 0.35 K cooling due to sulphates over the 1996–2046 period is eliminated altogether (making the contours in Fig. 4 vertical), the best-guess net warming over this period increases by 0.2 K, or about 20% (less than 0.35 K because the best-guess scaling on the sulphate signal in Fig. 4 is 0.6), whereas the upper bound on the 5–95% range increases by almost 50% to 1.7 K. This would also be the case for other factors, such as stratospheric ozone depletion, whose influence on climate is less easy to detect than the agents considered here[20], but in which trends are also expected to reverse over the next few years.

Thus far, we have assumed that the observed record consists only of anthropogenic signals and internal variability. Although this assumption is consistent with the available data[11,20,25], we have reason to expect that natural external factors have also affected temperatures over the twentieth century[10,11,26]. If we include the combined response (as estimated by HadCM2[11]) to solar variability and volcanic aerosols in a three-way fingerprint analysis[21], the uncertainty range in projected anthropogenic warming (eighth bar in Fig. 1) is almost unchanged. This is because the inclusion of this estimate of the natural signal does not have a detectable impact on the estimated amplitude of the anthropogenic signal (the use of decadal mean data minimizes the impact of individual volcanic eruptions and the 11-year solar cycle). Nevertheless, uncertainty in the fraction of recent warming attributable to natural versus anthropogenic influences, together with uncertainty in future natural forcing, remain important caveats.

We have focused on uncertainty in the climate system's response to a given profile of future greenhouse gas concentrations: uncertainty in other sources and sinks[27] and in future emissions[28] are also important. For example, the spread of responses by 2046 of a single climate model to the full range of scenarios considered by the IPCC Special Report on Emissions Scenarios (SRES)[28] is almost as large as the uncertainty in the response to a single scenario shown in Fig. 3. Not all of the SRES emissions scenarios, however, are based on explicit social and economic models[29], so it remains debatable whether uncertainty in future emissions is yet comparable to uncertainty in the response. Nevertheless, a quantitative assessment of the range of possible responses to a given emission path will increasingly be required to replace the best-guess projections hitherto provided by A–OGCMs. The approach described here provides a means of incorporating information on observed climate change into these ranges, until full-scale ensemble climate prediction systems become available[18]. A 5–95% range of 1–2.5 K above pre-industrial values by the 2040s under the IS92a scenario represents a first assessment, subject to various assumptions. We can expect this range to increase as these assumptions are relaxed in future work, but we can also expect it to be reduced if the observed

climate change signal continues to strengthen over the next few years. □

Methods

HadCM2-GS[16] and GFDL-GS[15] simulations are based on 4- and 5-member ensembles respectively forced with observed greenhouse gas and parametrized direct sulphate forcing to 1990 followed by 1% yr^{-1} compound increase in CO_2 (close to the IS92a scenario in terms of radiative forcing[23]) and IS92a projected sulphate loadings. ECHAM3-GS two-member ensemble[13] and ECHAM4-GS single simulation[14] are both based on observations followed by IS92a; the ECHAM4-GS1 single stimulation includes the impact of indirect sulphate forcing and tropospheric ozone changes. Model–observation comparison is based on decadal mean near-surface temperatures over the period 1946–96. Data are expressed as departures from the 1896–1996 mean, exploiting the fact that recent decades have been generally warmer than the preceding half-century without attempting to fit the details of surface temperature changes in poorly-sampled earlier decades. Ensemble members and 100-year segments of the control were masked with the pattern of missing data in the observations before computing means and anomalies, filtered to retain only scales greater than 5,000 km (refs 11, 30) and projected onto the 10 leading modes of internal spatio-temporal variability of the individual model control simulations (ECHAM3 control used for ECHAM4). Scaling factors (diamond/square ratios in Fig. 3) are estimated using standard optimal fingerprinting[19] modified to account for the presence of sampling noise in model-simulated signals[31,32]. Uncertainty estimates reflect uncertainty in scaling factors given interdecadal variability in the individual model control simulations (HadCM2: 1,700 years, ECHAM3: 1,900 years, GFDL: 1,000 years). In each case the first half of the control was used to define the detection space and for optimization, the second for uncertainty analysis.

Received 30 December 1999; accepted 2 August 2000.

1. Morgan, M. G. & Keith, D. W. Subjective judgements by climate experts. *Environ. Policy Anal.* **29,** 468–476 (1995).
2. Hansen, J. *et al.* Climate response times: dependence on climate sensitivity and ocean mixing. *Science* **229,** 857–859 (1985).
3. Raper, S. C. B., Wigley, T. M. L. & Warrick, R. A. in *Rising Sea Level and Subsiding Coastal Areas* (eds Millman, J. D. & Haq, B. U.) 11–45 (Kluwer Academic, Norwell, Massachusetts, 1996).
4. Wigley, T. M. L., Jones, P. D. & Raper, S. C. B. The observed global warming record: What does it tell us? *Proc. Natl Acad. Sci.* **94,** 8314–8320 (1997).
5. Forest, C. E., Allen, M. R., Stone, P. H. & Sokolov, A. P. Constraining uncertainties in climate models using climate change detection techniques. *Geophys. Res. Lett.* **27,** 569–572 (2000).
6. Meehl, G. A., Boer, G. J., Covey, C., Latif, M. & Stouffer, R. J. The Coupled Model Intercomparison project (CMIP). *Bull. Am. Meteorol. Soc.* (in the press).
7. Santer, B. D. *et al.* A search for human influences on the thermal structure of the atmosphere. *Nature* **382,** 39–46 (1996).
8. Hegerl, G. C. *et al.* Detecting greenhouse gas-induced climate change with an optimal fingerprint method. *J. Clim.* **9,** 2281–2306 (1996).
9. Hegerl, G. *et al.* On multi-fingerprint detection and attribution of greenhouse gas and aerosol forced climate change. *Clim. Dyn.* **13,** 613–634 (1997).
10. North, G. R. & Stevens, M. J. Detecting climate signals in the surface temperature record. *J. Clim.* **11,** 563–577 (1998).
11. Tett, S. F. B., Stott, P. A., Allen, M. R., Ingram, W. J. & Mitchell, J. F. B. Causes of twentieth century temperature change near the Earth's surface. *Nature* **399,** 569–572 (1999).
12. Johns, T. C. The Second Hadley Centre coupled ocean-atmosphere GCM: model description, spin-up and validation. *Clim. Dyn.* **13,** 103–134 (1997).
13. Voss, R., Sausen, R. & Cubasch, U. Periodically synchronously coupled integrations with the atmosphere-ocean general circulation model ECHAM3/LSG. *Clim. Dyn.* **14,** 249–266 (1998).
14. Röckner, E., Bengtsson, L., Feichter, J., Lelieveld, J. & Rodhe, H. Transient climate change simulations with a coupled atmosphere-ocean gcm including the tropospheric sulfur cycle. *J. Clim.* **12,** 3004–3032 (1999).
15. Knutson, T. R., Delworth, T. L., Dixon, K. W. & Stouffer, R. J. Model assessment of regional surface temperature trends (1949–1997). *J. Geophys. Res.* **104,** 30981–30996 (1999).
16. Mitchell, J. F. B., Johns, T. C., Gregory, J. M. & Tett, S. F. B. Climate response to increasing levels of greenhouse gases and sulphate aerosols. *Nature* **376,** 501–504 (1995).
17. Sokolov, A. P. & Stone, P. H. A flexible climate model for use in integrated assessments. *Clim. Dyn.* **14,** 291–303 (1998).
18. Allen, M. R. Do-it-yourself climate prediction. *Nature* **401,** 642 (1999).
19. Hasselmann, K. On multifingerprint detection and attribution of anthropogenic climate change. *Clim. Dyn.* **13,** 601–611 (1997).
20. Allen, M. R. & Tett, S. F. B. Checking internal consistency in optimal fingerprinting. *Clim. Dyn.* **15,** 419–434 (1999).
21. Stott, P. A. Attribution of twentieth century climate change to natural and anthropogenic causes. *Clim. Dyn.* (in the press).
22. Wood, R. A., Keen, A. B., Mitchell, J. F. B. & Gregory, J. M. Changing spatial structure of the thermohaline circulation in response to atmospheric CO_2 forcing in a climate model. *Nature* **399,** 572–575 (1997).
23. Mitchell, J. F. B. & Johns, T. C. On modification of global warming by sulphate aerosols. *J. Clim.* **10,** 245–266 (1997).
24. Corti, S., Molteni, F. & Palmer, T. N. Signature of recent climate change in frequencies of natural atmospheric circulation regimes. *Nature* **398,** 799–802 (1999).
25. Delworth, T. L. & Knutson, T. R. Simulation of early 20th century global warming. *Science* **287,** 2246–2250 (2000).
26. Cubasch, U., Voss, R., Hegerl, G. C., Waszkewitz, J. & Crowley, T. J. Simulation of the influence of solar radiation variations on the global climate with an ocean-atmosphere general circulation model. *Clim. Dyn.* **13,** 757–767 (1997).
27. Cox, P. M., Betts, R. A., Jones, C. S., Spall, S. A. & Totterdell, I. J. Acceleration of global warming due to carbon-cycle feedbacks in a 3D coupled model. *Nature* (submitted).
28. Intergovernmental Panel on Climate Change *Special Report on Emissions Scenarios* (eds Nakićenović, N. & Swart, R.) (Cambridge Univ. Press, 2000).
29. Smith, S. J., Wigley, T. M. L., Nakicenovic, N. & Raper, S. C. B. Climate implications of greenhouse gas emissions scenarios. *Technol. Forecast. Social Change* (in the press).
30. Stott, P. A. & Tett, S. F. B. Scale-dependent detection of climate change. *J. Clim.* **11,** 3282–3294 (1998).
31. Ripley, B. D. & Thompson, M. Regression techniques for the detection of analytical bias. *Analyst* **112,** 377–383 (1987).
32. van Huffel, S. & Vanderwaal, J. *The Total Least Squares Problem: Computational Aspects and Analysis* (Society for Industrial & Applied Mathematics, Philadelphia, 1991).

Acknowledgements

We thank T. Barnett, C. Forest, N. Gillett, K. Hasselmann, G. Hegerl, W. Ingram, G. Jones, S. Raper, B. Ripley, S. Smith, A. Sokolov, P. Stone, S. Tett, I. Tracey and A. Weaver for suggestions. This work was supported by the UK Natural Environment Research Council (M.R.A.); The UK Department of Environment, Transport and Regions (P.A.S.); the UK Meteorological Office's Research and Development Programme (J.F.B.T.); the European Commission (R.S.); and the US National Oceanic and Atmospheric Administration (T.L.D.); with additional support from the US Department of Energy and the British Council.

Correspondence and requests for materials should be addressed to M.R.A. (e-mail: m.r.allen@rl.ac.uk).

Pressure-induced changes in the compression mechanism of aluminous perovskite in the Earth's mantle

John P. Brodholt

Department of Geological Sciences, University College London, Gower Street, London WC1E 6BT, UK

Although aluminium is the fifth most abundant element in the Earth's mantle, its effect on the physical properties of perovskite, the main mineral phase in the lower mantle, has largely been ignored. It is becoming clear, however, that many properties of $MgSiO_3$ perovskites are remarkably sensitive to small amounts of aluminium[1–4]. In particular, perovskite with only 5 wt% Al_2O_3 has a bulk modulus 10% lower than that of the pure magnesian end-member[12]. The increased compressibility may be due to the high concentrations of oxygen vacancies required to balance the charge of the aluminium[5]; if so, this would have important consequences for the mantle, as aluminous perovskites could be weaker, have lower seismic velocities and be hosts for water. To test whether oxygen vacancies exist in aluminous perovskites, I have calculated the compressibility of end-member defect-bearing perovskites using *ab initio* methods. The results show that perovskites with oxygen vacancies do have significantly greater compressibilities than those without such vacancies. But the results also suggest that oxygen vacancies become unfavourable at high pressures, in which case only the physical properties of the shallow lower mantle would be affected by aluminium—with the deeper mantle retaining properties similar to those of aluminium-free perovskite.

Two substitution mechanisms have been proposed for the incorporation of Al^{3+} into $MgSiO_3$ perovskite. The first is the coupled substitution $2Al^{3+} \rightarrow A\dot{l}_{Mg} + Al'_{Si}$ (ref. 6) where aluminium enters both cation sites (the M site normally occupied by 2+ cations, and the octahedral site normally occupied by silicon) and does not require the creation of vacancies for charge balance. (Here the $\dot{}$ and $'$